Thermophysical Characterisation of ZrC_xN_y Ceramics Fabricated via Carbothermic Reduction-Nitridation

R. Harrison, O. Ridd, D.D. Jayaseelan, W.E. Lee

Department of Materials, Imperial College, London, SW7 2AZ, UK

Abstract

Thermophysical properties of ZrC_xN_y ceramics prepared from powders produced via a two-step carbothermic reduction-nitridation of zirconia were characterised to 2200K. Preliminary evidence for the mechanism of nitridation shows a gas-solid phase reaction at the ZrC particle surface which is the first such observation with this system. Electrical and thermal conductivities were higher than commercially available ZrC and ZrN. Thermal conductivity values of the ZrC_xN_y phases at room temperature were between 35–43 $Wm^{-1}K^{-1}$, increasing with nitrogen content due to increased electronic contribution to thermal conduction and increased to 40–50 $Wm^{-1}K^{-1}$ with temperature. Electrical conductivity also increased with nitrogen content and values were in the range of 100–450 x $10^4\Omega^{-1}m^1$, but decreased with increasing temperature showing metallic behaviour.

Keywords: Nuclear fuel, Inert Matrix Fuel, Carbide, Zirconium Nitride, Carbonitride, Thermal Conductivity, Specific Heat, Electrical Conductivity

1. Introduction

Carbide and nitride fuels are being considered for application in Generation IV reactors, space power reactors and accelerator driven systems (ADS) [1–3]. Fuel materials used in the Gas Cooled Fast Reactor (GFR) nuclear power plant will need to withstand higher temperatures (in the region of 1273-1873K) [4], harsher radiation fields due to the hardened neutron spectrum and possess increased thermophysical properties to increase efficiency of heat transfer in the reactor. Non-oxide fuels contain fewer lighter elements per heavy metal, i.e. MN compared to MO_2 (M=metal) giving a higher heavy metal density and therefore a higher fissile density which is ideal for use in fast breeder reactors in maintaining a fast neutron spectrum [5]. Recent work has focused on assessing thermophysical properties, such as heat capacity, thermal expansion and thermal conductivity of actinide nitrides, inert matrix candidates and their composites in order to predict the in-pile behaviours of nitride fuels [6].

Zirconium nitride is being considered for use as an inert matrix fuel (IMF) or as advanced fuel particle coatings due to its high thermal conductivity, low neutron capture cross section and chemical compatibility with existing fuel cycle technology [7]. Due to this increased interest recent work has focused on assessing thermophysical properties of ZrN and mixed phases of actinide nitrides dispersed in ZrN [8–14].

The carbothermic reduction-nitridation of oxide powders is an attractive route for the large scale production of non-oxide fuels [12]. Methods of carbothermal reduction-nitridation of oxides

Email address: R.Harrison11@Imperial.ac.uk (R. Harrison)

generally use similar processing parameters [6, 15], mixing of oxide powder with a carbon source, heat treatment to between 1800-2300K under inert atmosphere and then further heat treatment in a hydrogen doped nitrogen atmosphere to complete the reaction and remove excess carbon. The basic mechanism of carbothermic reduction-nitridation is;

$$ZrO_2 + 3 - xC \longrightarrow ZrC_{1-x} + 2CO \tag{1}$$

$$ZrC + \frac{1}{2}N_2 + 2H_2 \longrightarrow ZrN + CH_4 \tag{2}$$

This process can however leave impurities, such as carbon, oxygen and vacancies and the effects on the thermophysical properties of bulk ZrN need to be assessed to produce accurate values of thermal and electrical conductivity. There is much scatter in published data due to limited reporting of purity and stoichiometry [8, 10, 13, 16–18]. Mixed phase zirconium carbonitrides and sub-stoichometric ZrN are typically produced using magnetron sputtering or chemical vapour deposition techniques to achieve control over the final product [19–22]. However, group IV carbonitrides have been fabricated in bulk by milling together commercially available MC and MN powders in desired ratio's before sintering [23]. In this work the carbothermal reduction-nitridation process was used to fabricate powders of ZrN and ZrC_xN_y from ZrO_2 to minimise and examine the effects that impurities such as oxygen, carbon and vacancy defects may have on the thermophysical properties of bulk ZrN, ZrC and ZrC_xN_y ceramics.

2. Experimental

Powders of ZrO_2 (Sigma Aldrich, Gillingham, UK) and C (ABCR, Karlsruhe, Germany) were mixed in a ratio as to achieve a C/Zr molar ratio of 2.7 and 3.0 (sample names, 1Zr-2.7C and 1Zr-3C respectively). These mixtures were homogenised by ball milling a slurry (in acetone) for 12h using ZrC milling media and dried at 363K. Powders were then subject to a 4h dwell at 2073K (+10K/min) under Ar in a graphite furnace (Fine ceramics technologies (FCT) systeme GmbH, Frankenblick, Germany) to produce the corresponding carbides by carbothermal reduction. The resulting powders were then ball milled for 12h in acetone using ZrC and dried as before. Nitridation of dried powders were carried out for 4–24h at 1800–1873K (+35K/min) under a flowing atmosphere of 10% H_2- 90% N_2 gas in a tube furnace (50 mm internal diameter and 1200 mm long, flow rate of 0.5 L/min, Lenton, Derbyshire, UK).

Four of the as-fabricated ZrC_xN_y powders (sample names ZrCN1-4, table 1), commercially-available ZrC (Sigma Aldrich, 5 μm, $\geq$ 99.95%) and ZrN (Sigma Aldrich, 1-2 μm, $\geq$ 99.0%) were densified using hot pressing (HP W/25/1, FCT systeme) in a graphite die (20mm diameter), under argon (1 Bar, static atmosphere). Sintering was carried out for 1 h at 2273K (+10K/min) under 50 MPa uniaxial pressure. Ranges of powder sizes and grain sizes in the ceramics were measured by SEM, density was measured by the Archimedes method and the reported value is the mean of three measurements with the error given as the standard deviation of this measurement. Combustion analysis of carbon content was performed using combustion and Infra-Red (IR) detection of the resulting CO/CO_2 gas (Horiba, EMIA-V2 series, Kyoto, Japan) with oxygen and nitrogen content being measured using a separate instrument, detecting oxygen as CO/CO_2 by two non-dispersive IR detectors and nitrogen by thermal conductivity (Horiba, EMGA-930). For oxidation analysis the samples were oxidised at 1173K in air and the resultant gases detected by IR and thermal conductivity (Thermofisher, Loughborough, UK), however oxygen was not detected. Errors in the chemical analysis are reported as the average of three measurements and the error given as the standard deviation of those measurements. High resolution transmission electron microscope analysis was performed on the powders using bright field (BF) imaging and

selected area electron diffraction (SAED) (HRTEM FX2100, JEOL, Japan), lattice planes were indexed by calculating the d_{hkl} values from the reciprocal of the separation of diffraction spots. Microstructure and phase characterisation of the sintered and polished pellets were performed using back scattered electron imaging (SEM, JSM 5610, JEOL, Hertfordshire, UK). Phase analysis was done using X-ray diffraction (XRD) (Pananalytical, The Netherlands) at 40 kV and 40 mA, using Ni-filtered CuKα radiation. Lattice parameters were calculated using the interplanar spacing d_{hkl} of 5 reflections using Bragg's law in equation 3 (where λ is the X-ray wavelength of 1.5406 Å and θ is the angle of between the X-ray and the diffraction plane), for a cubic unit cell the lattice parameter α, is given below (equation 4). Systematic error was accounted for using the Nelson-Riley function (equation 5), uncertainty in the lattice parameter was $\pm$0.001 Å.

$$\lambda = 2d_{hkl}sin\theta \tag{3}$$

$$\alpha = d\sqrt{h^2 + k^2 + l^2} \tag{4}$$

$$\delta\theta = \frac{cos^2\theta}{sin\theta} + \frac{cos^2\,\theta}{\theta} \tag{5}$$

Thermal diffusivity was measured using the laser flash technique (LFA-427, Netzsch GmbH, Wolverhampton, UK) from room temperature to 2073K under high purity Ar (99.99%). A laser pulse (voltage: 450V for 0.8 ms) was shot onto the front face of the sample ($\sim$1 mm thick). An IR detector was used to measure the temperature from the sample rear face. Heat capacity was measured using differential scanning calorimetry (DSC, STA449-C, Netzsch) from room temperature to 1273 K (+20 K/min, 50ml/min) under argon atmosphere (99.999% pure) using a zirconium oxygen trap system in the furnace. The samples were cylindrical pellets with 5mm diameter and 1mm tall. A sapphire reference was used for calibration. The manufacturers state the accuracy of the instrument at $\pm$3% which were reported as the error of the measurements. Thermal conductivity was calculated from the experimental values obtained for the thermal diffusivity, heat capacity and density using equation 6, where K is the thermal conductivity ($Wm^{-1}K^{-1}$), α is the thermal diffusivity (m^2s^{-1}), ρ is the density (kg m^{-3}) and Cp is the heat capacity (J kg^{-1} K^{-1}). Errors for the thermal conductivities of the samples are reported as a propagation of the errors from the densities, thermal diffusivities and heat capacities.

$$K = \alpha\rho Cp \tag{6}$$

Electrical conductivity was measured using four point DC between 273-1023K under flowing high purity argon (99.99% pure, 50mL/min) between platinum electrodes. Electrical conductivity ($10^4\Omega^{-1}m^1$) was calculated from the inverse of Ro, where Ro represents the resistance of a length of material. Ro (Ωm) was determined using equation 7, where V is the measured voltage (V), I is the applied current (Amps), A is the cross sectional area of the sample (cm^2) and L is the length (cm). Values of electrical conductivity were reported as the average of two measurements taken by reversing polarity of the current, errors were reported as the propagation of error from the standard deviation of two measurements along with errors in the cross sectional area measurements. Each sample was confirmed to obey Ohms law by plotting voltage as a function of current (currents between -100 to +100 mA) with all samples showing linear behaviour and an R^2 value of $\geq$ 0.9999.

$$Ro = \frac{V}{I} \times \frac{A}{L} \tag{7}$$

3. Results and Discussion

3.1. Powder Fabrication

Chemical analyses of carbon, oxygen and nitrogen using the oxidation technique are presented in table 1, and analyses from combustion in table 2. In both tables the at% C decreases with increasing dwell times and temperatures. The stoichiometries of the samples do not give a ZrC_xN_y composition where x+y=1, however this is a common trait of transition metal carbides and nitrides, as they can accommodate a range of vacancy defects [16]. The vacancies may have also been produced by an incomplete nitridation whereby carbon was removed from the particle but was not replaced by a nitrogen. The chemical analyses presented in table 1 were performed on the powder samples after reaction, however in table 2 the pellets were ground with a pestle in a mortar in air. From both chemical analyses (tables 1 and 2) it can be seen that the increasing reaction time does not result in a proportional increase in nitrogen content of the sample, indicating that the rate of nitridation is decreasing as the reaction proceeds. This decrease in rate would be expected, as the reaction proceeds there is less surface area of the ZrC particle to react with and the diffusion length for both carbon leaving the particle and nitrogen entering the particle increase.

The presence of oxygen in the samples may be due to contamination from the grinding in air or also an error in the instrument where air is trapped between the particles and provides false detection, however trapped air would also lead to the detection of nitrogen which may explain the nitrogen observed in the samples 1Zr3C, 1Zr2.7C and the commercial ZrC powder in table 1. The increase in oxygen content with sintering time suggests the material is undergoing some oxidation during nitridation. The two chemical analyses are however in good agreement proving similar stoichiometries for the ceramics that were produced from hot pressing, meaning there was limited, if any, carbon ingress from the graphite dies used to produce the pellets.

Figure 1 reveals the powders are crystalline cubic materials, however there are asymmetric peaks corresponding to a composite material, looking at the {311} and {222} reflections a shoulder of the peak can be observed on the left corresponding to ZrC which decreases as carbon content decreases and the ZrN peak being the dominant peak on the right, which increases in relative intensity as nitrogen content increases. After prolonged dwell times the ZrN peak increases relative to a decrease in the ZrC peak. From this it can be seen that increased dwell times and higher dwell temperatures give greater nitridation.

Bright field transmission electron microscopy (BF-TEM) of a ZrC_xN_y powder after nitridation at 1800K for 8h with a chemical composition of $ZrC_{0.67}N_{0.33}$ (figure 2) reveals a core-rim particle structure (2c), which is evidence for a gas-solid surface reaction mechanism. The SAED pattern of the particle (figure 2d) reveals a single crystalline pattern of ZrN ($< 112 >$zone axis) along with additional satellite streaks which were observed consistently for the sample. The lattice constants for ZrC and ZrN are within 2.6% of each other and both crystals are cubic ($Fm\overline{3}m$) so distinguishing by electron diffraction is difficult. The satellite peaks associated with $< 112 >$ pattern spots could be due to diffraction from a second phase which could be ZrC or ZrC_xN_y. The streaking could also arise from strain effects in the lattice such as modification of the unit cell parameter via carbon removal from the ZrC lattice and increasing vacancy defects and nitrogen content. Short range ordering of defects has been reported to cause diffuse streaking in SAD patterns [24], however sharp streaks have been attributed to severe deformation of the lattice by Swain and Hannick [25]. Strain in the crystal may also be from elastic strain effects from the orientations of the nitride layer on the carbide particle.

An initial evaluation of the TEM and XRD (figures 1 and 2) results along with the evidence of a decrease in rate of nitridation as the reaction proceeds suggest the ZrC particle is destabilised by the hydrogen at the particle surface leading to a ZrC_{1-x} phase. Bardelle and Warin [26]

have measured the presence of HCN and not CH_4 by gas-chromatography mass spectrometry of the furnace exhaust gas and suggest that the reaction mechanism proceeds by the formation of HCN during the carbothermic reduction-nitridation of (U,Pu)O_2 which then reacts further with the carbide increase the progress of nitridation. The vacancies in this sub-stoichiometric phase are then replaced with nitrogen, forming an initial $ZrC_{1-x}N_x$ layer. The destabilisation of the ZrC_{1-x} phase and replacement with nitrogen continues until there is a surface layer of ZrN, a reaction layer under the surface of $ZrC_{1-x}N_x$ and a core of ZrC. Existence of two monolithic ZrN and ZrC phases as well as a $ZrC_{1-x}N_x$ reaction layer is also indicated by the peaks observed from XRD (figure 1). This preliminary evidence of a gas-solid phase reaction at the surface of the particle is the first report of such a mechanism in this system. This is unlike other studies on similar reaction systems, such as carbothermal reduction of ZrO_2 to ZrC and the one step carbothermal reduction-nitridation of SiO_2 to Si_3N_4 which undergo gas-gas phase reaction mechanisms at nucleation points separate from the particle's surface [27–29].

3.2. Sintering and Characterisation

XRD of the ceramic pellets (figure 3) revealed sharper single peaks from highly crystalline phases, showing that during sintering a solid solution is formed. The formation of a solid solution is an effect of the sintering/annealing reducing the residual strain in the lattice and allowing diffusion of the nitrogen throughout it. The nitrides degree of covalent bonding is less than the carbide due to it possessing an extra valence electron which occupies an anti-bonding orbital. This decreased covalency would increase the diffusion rate of nitrogen giving the solid solution after sintering of ZrC_xN_y phases. It is important to note that if the XRD had been performed on the pellet only, then the solid solution may have been mistaken for a pure single phase with a slight deviation from lattice parameter. Account must be taken of changes from powders to dense ceramics in the fabrication of non-oxides via the carbothermic reduction-nitridation route. Lattice parameters calculated from the XRD pattern of the ceramics (figure 3) show a decrease with increasing nitrogen content. Plotting lattice parameter (figure 4) as a function of [C]/[C]+[N] (where [C] and [N] are the x and y stoichiometry values respectively of the ZrC_xN_y phases) with published values of ZrC and ZrN lattice parameter gives good correlation showing agreement between the chemical analysis and XRD data [30, 31].

Distinct colour changes were observed in the pellets produced from the ZrC_xN_y phase (figure 5). As nitrogen content increases the samples become lighter changing from a grey colour through orange and red to yellow-gold, as previously observed by Lengauer [32]. Backscattered electron images (figure 6a) of the ZrN ceramic produced from commercial powder reveal it is near fully dense, with larger grains of around 100 μm compared to the ZrC sample (figure 6b) produced using commercial powders which has around 8 vol% porosity and small grains of around 5-10 μm diameter. The difference between densities could be an effect of the initial starting powders as the manufacturers analysis gave the ZrN particle size at 1-2 μm and the ZrC as 5 μm. The carbide is difficult to sinter due to strong covalent bonds resulting in slow diffusion of carbon through the sample. The nitride also contains strong covalent bonding but as it has an extra valence electron, more of its anti-bonding states are occupied, reducing the strength of the covalent bond which may explain the increased density of the nitride over the carbide, this improved sintering of the carbonitrides could provide a way to achieve high density ZrC samples if the effect is observed at low wt% N. The difference in grain size between the two samples of ZrN and ZrC is most likely due to the nitride undergoing more grain growth during the 1 h dwell. Figure 6c shows the surface microstructure of the pellet produced from the zirconium carbonitride phase $ZrC_{0.55}N_{0.4}$. Less grain growth is observed than in the nitride, however it contains much larger grains ($\sim$30 μm), than the carbide ($\sim$5 μm) and is a mixture of the two grain sizes seen in figures 6a and 6b. The sample is also fully dense with no porosity observed

by SEM, evidence that the nitrogen content has had a positive impact on the sinterability of the samples. The densities of the ceramics are given in table 3 along with the starting particle and average grain sizes. The density of the ZrC_xN_y phases increases with increasing nitrogen content, from around 6.90 g/cm^3 to 7.06 g/cm^3 and it is expected that the carbonitrides are an intermediate value of ZrC and ZrN according to the rule of mixtures.

3.3. Thermophysical Analysis

Figure 7 shows that the thermal diffusivity of the ZrC_xN_y pellets is higher than both the ZrC and ZrN pellets fabricated from the commercially available powders (referred to as ZrC com and ZrN com from here on). A general trend of increasing thermal diffusivity with increasing nitrogen content can be observed agreeing well with Lengauer et al. [23], however due to slight differences in densities the $ZrC_{0.4}N_{0.55}$ and $ZrC_{0.33}N_{0.6}$ slightly decrease in thermal diffusivty. It might be expected if the trend is continued, that ZrN would have a higher thermal diffusivity than ZrC, however the low thermal diffusivity of the commercial ZrN sample may be due to the purity of the sample. The thermal diffusivity of ZrC may be slightly less than expected due to the ∼8% porosity of the samples (table 3).

Heat capacities of single phase ZrC and ZrN from the National Institute of Standards and Technology (NIST) data (figure 8) shows the two phases have similar heat capacities and vary by no more than about 0.05 J/g K at their maximum deviation [33]. Figure 8 also shows the experimentally obtained heat capacities from the ceramics prepared in this work which compare well with values for ZrC and ZrN from NIST to around 1200K. Heat capacity values for the ZrC_xN_y phases were calculated using the rule of mixtures based on wt%N and wt%C from the literature [33] up to 2200 K to determine the thermal conductivity of the ceramics from measured thermal diffusivities. Error ranges were added to the calculated values so the calculated values of the ZrC_xN_y phases would fall within the range of single phase ZrC and ZrN.

Experimentally obtained thermal conductivities of the ZrC and ZrN pellets matched well with previous work (figure 9) [8, 10, 17, 32, 34, 35]. Thermal conductivity data from all literature values have been corrected corrected to 100% TD for comparison using the Maxwell-Eucken equation (equation 8), where P is the porosity, K_p is the measured thermal conductivity, K_{TD} is the thermal conductivity of a fully dense material [36]. The ZrC samples in this work are slightly lower than Hedge et al. [35] however this is due to it having around 8% porosity. The ZrN sample agrees well with the previous work and is slightly higher than Neel et al. [34] and Hedge et al. [17] however Basini et al.'s [10] corrected values are much higher, this may be due to the extrapolation of thermal conductivity using the Maxwell-Euken equation for a 70%TD (shown in figure 9) sample being inappropriate. The thermal conductivity values for the highest N content sample reported by Lengauer et at. [23] is shown in figure 9 and is much higher than values reported for ZrN.

$$Kp = \left(\frac{1-P}{1+P}\right) K_{TD} \tag{8}$$

Figure 10 reveals a higher thermal conductivity for all ZrC_xN_y phases as compared to the ceramics produced using commercial ZrC and ZrN, only the commercial ZrC sample has been corrected to 100%TD using equation 8. Figure 10 shows an almost double increase between $ZrC_{0.12}N_{0.78}$ and ZrC, and a 4 fold increase compared with ZrN respectively at room temperature. This difference between the ZrC_xN_y phases and the ZrC ceramics is due to the differences in thermal diffusivity and density. Heat capacities for the materials are similar, however the ZrC_xN_y phases have a higher thermal diffusivity than ZrC and a density similar to ZrN so that the resultant thermal conductivity data is not a mixture of the two monolithic end materials, but

higher than them. Lengauer et al. [23] observed a similar trend with thermal conductivity increasing with increasing nitrogen content from room temperature to 1000K, reporting $ZrC_{0.25}N_{0.75}$ and $ZrC_{0.11}N_{0.89}$ ceramics having room temperature thermal conductivities of around 25 and 30 $Wm^{-1}K^{-1}$ respectively. This is explained as the transition metal carbides have a lower density of states at the Fermi level than the corresponding nitrides, and so their electrical and thermal conductivities are lower [32], however in the same text they quote room temperature thermal conductivity of ZrC higher than ZrN around 25 and 10 $Wm^{-1}K^{-1}$ respectively (figure 9) which may be due to the scatter in the thermal conductivity of these materials. The increase in conductivity of the samples in this work compared with that of Lengauer et al. [23] may be due to the processing route used. Lengauer et al. [23] mixed commercially available ZrC and ZrN to form the ZrC_xN_y phases, which may contain impurities. Impurities, such as oxygen, within the sample will lead to increasing phonon and electron scattering at the impurity, decreasing thermal conductivity. Effects of oxygen on sintering and thermophysical properties of ZrN have been discussed by Pukari and Takano [37] and Stanek et al. [38] and the unavoidable oxygen impurities present in the samples of around 2-5 at%O (table 2) from processing methods will have a detrimental effect on the thermal conductivities of the samples (figure 10). The low values of thermal conductivity for the commercial ZrN pellet in this work may also be attributed to oxygen impurities or vacancies being present in the starting powder, and although it does seem to match well with previous literature the bulk of experimental data is from commercially available ZrN [8, 10, 13, 18]. From the trend observed in this work it would be expected that pure ZrN samples should have room temperature thermal conductivities greater than 45–50 $Wm^{-1}K^{-1}$, which would be around 4 times higher than some values reported in the literature (figure 9). Adachi et al. [13, 18] measured the thermal conductivity of commercial available ZrN using spark plasma sintering to fabricate ceramics with densities of 82.3 and 91.2% T.D. and reported room temperature thermal conductivities of about 20 and 30 $Wm^{-1}K^{-1}$ K^{-1} respectively, correcting this to 40 $Wm^{-1}K^{-1}$ K^{-1} for a fully dense ceramic using the Maxwell-Eucken equation.

Electrical conductivity was measured using 4 point DC to observe the electronic contribution to the thermal conductivity to fully characterize the mechanism of thermal conductivity in these ceramics. The thermal conductivity of a material is the sum of heat transfer via lattice vibrations, known as phonons and electrical conductivity as show in equation 9.

$$K_{Total} = K_{Lat} + K_{el} \tag{9}$$

The electronic contribution, K_{el} can be determined using the Wiedemann-Franz-Lorenz equation (equation 10), where L is the Lorenz number (2.44 x $10^4\Omega^{-1}m^1$) [13], σ is the electrical conductivity ($\Omega^{-1}m^{-1}$) and T is the absolute temperature (K)

$$K_{el} = \sigma L \mathrm{T} \tag{10}$$

Figure 11 shows the electrical conductivity decreases with temperature but increases with increasing nitrogen content, although the commercial powder is far lower than the samples produced from the fabricated powders. Adachi et al. [13] reported the electrical conductivity of a ZrN sample with about 8% porosity at room temperature to be around 200 x $10^4\Omega^{-1}m^1$ decreasing with temperature and corrected this to 300 x $10^4\Omega^{-1}m^1$for a fully dense sample. Electrical conductivity of ZrC matched well with previous data [16]. Lengauer et al. [23] reported the room temperature electrical conductivity of the carbonitrides to be in the range of 200–450 x $10^4\Omega^{-1}m^1$, with conductivity increasing with nitrogen content. Figure 12 shows the electronic contribution, K_{el} (calculated from equation 10), increases with absolute temperature and also increases with increasing nitrogen content, whereas the phonon contribution (K_{lat}, estimated using equation 9) decreases with temperature and increasing nitrogen content (figure 12).

The percentage of the thermal conductivity at room temperature that comes from electrical conductivity (table 4) shows that the dominant mechanism for thermal conduction in samples with higher nitrogen content is via electron heat transfer (K_{el}). This agrees with Lengauer et al.'s statement that the density of states at the Fermi level in the nitrides is lower than the carbides [32]. Nitrogen also possesses an extra electron in its 2p orbital compared with carbon which would occupy an antibonding orbital located above the Fermi energy leading to increased electrical conductivity. The reduced electrical contribution to thermal conductivity in the ZrN sample may again be due to vacancy or oxygen impurities causing poor conduction.

4. Conclusions

Mixed phases ZrC_xN_yceramics were produced using the established carbothermic reduction and nitridation process. Increasing temperature and dwell times of the nitridation process increased nitrogen content in the ceramics, however they all still contained carbon even at long dwell times of 24 h. A carbonitride phase may also be a desirable composite for nuclear fuels as it would combine advantages from both monolithic phases, such as good fission product retention of ZrC [16], with the higher achievable densities, improved radiation damage tolerance and compatibility with current reprocessing techniques of ZrN [6, 39]. TEM showed the formation of a nitride layer on the ZrC particle, this explains the long dwell times needed to achieve higher nitrogen content due to increased time for nitrogen diffusion into the core of the particle. Thermophysical characteristics of these ZrC_xN_y ceramics have been evaluated with thermal conductivities of around 35 $Wm^{-1}K^{-1}$ for the lowest nitrogen containing samples and 43 $Wm^{-1}K^{-1}$ for the highest nitrogen containing sample, this increased with temperature for all samples. The thermal conductivity results obtained in this study are much higher than those previously reported, with room temperature values for commercially available ZrN being around 10 $Wm^{-1}K^{-1}$, this may be due to the processing route used to fabricate the powders leading to a purer powder and pellet production route which led to fully dense pellets. Electrical conductivities of the mixed ZrC_xN_y phases were in the range of 250–500 x $10^4\Omega^{-1}m^1$ and decreased with increasing temperature indicating metallic like behaviour. The proportion of electrical conductivity contribution to thermal conductivity, K_{el}, increases with increasing nitrogen content. Zirconium carbide and zirconium nitride both offer benefits as use as inert matrix fuel materials for next generation nuclear power plants. However, the scatter of thermophysical data for ZrN in the literature has led to reviews comparing inert matrix fuel candidates reporting the thermal conductivity of ZrN as much lower than the ZrC_xN_y phases presented in this work, sometimes with values of around 10 $Wm^{-1}K^{-1}$[40, 41]. It has also been shown that carbon contamination from the carbothermic reduction and nitridation route is present even after long sintering times and high temperatures, however all mixed phases had excellent thermal conductivity values.

Acknowledgments

The authors would like to thank colleagues at the European Ceramic Centre in Limoges for their help with TEM studies and combustion analyses, Dr A. Berenov for assistance with making electrical measurements and Mr Garry Stakalls for help with sample preparation using the hot press.

References

[1] Z. Su'Ud and H. Sekimoto. Design and safety aspect of lead and lead-bismuth cooled long-life small safe fast reactors for various fore configurations. *Journal of Nuclear Science and Technology*, 32(9):834–845, 1995.

[2] R. B. Matthews, K. M. Chidester, C. W. Hoth, R. E. Mason, and R. L. Petty. Fabrication and testing of uranium nitride fuel for space power reactors. *Journal of Nuclear Materials*, 151(3):345, 1988.

[3] Y. Arai and K. Minato. Fabrication and electrochemical behavior of nitride fuel for future applications. *Journal of Nuclear Materials*, 344(1-3):180–185, 2005.

[4] M. K. Meyer, R. Fielding, and J. Gan. Fuel development for gas-cooled fast reactors. *Journal of Nuclear Materials*, 371(13):281–287, 2007.

[5] W.E. Lee, M. Gilbert, S.T. Murphy, and R.W. Grimes. Opportunities for advanced ceramics and composites in the nuclear sector. *Journal of the American Ceramic Society*, 96(7):2005–2030, 2013.

[6] Y. Arai. *Nitride Fuel*, book section 3.02, pages 41–54. Comprehensive Nuclear Materials. Elsevier, Oxford, 2012.

[7] M. Burghartz, G. Ledergerber, H. Hein, R. R. van der Laan, and R. J. M. Konings. Some aspects of the use of ZrN as an inert matrix for actinide fuels. *Journal of Nuclear Materials*, 288(23):233–236, 2001.

[8] A. Ciriello, V. V. Rondinella, D. Staicu, J. Somers, O. Benes, R. Jardin, D. Bouxire, F. Wastin, and E. Colineau. Thermophysical characterization of ZrN and (Zr,Pu)N. *Journal of Alloys and Compounds*, 473(1-2):265–271, 2009.

[9] Y. Arai, M. Akabori, and K. Minato. Progress of nitride fuel cycle research for transmutation of minor actinides. In *Advanced nuclear fuel cycles and systems (GLOBAL 2007)*. American Nuclear Society, 2007. (Japan) [Japan Atomic Energy Agency - JAEA, Tokai-mura, Naka-gun, Ibaraki-ken, 319-1195].

[10] V. Basini, J. P. Ottaviani, J. C. Richaud, M. Streit, and F. Ingold. Experimental assessment of thermophysical properties of (Pu,Zr)N. *Journal of Nuclear Materials*, 344(1-3):186–190, 2005.

[11] Y. Arai and K. Nakajima. Preparation and characterization of PuN pellets containing ZrN and TiN. *Journal of Nuclear Materials*, 281(23):244–247, 2000.

[12] K. Minato, M. Akabori, M. Takano, Y. Arai, K. Nakajima, A. Itoh, and T. Ogawa. Fabrication of nitride fuels for transmutation of minor actinides. *Journal of Nuclear Materials*, 320(12):18–24, 2003.

[13] J. Adachi, K. Kurosaki, M. Uno, and S. Yamanaka. Effect of porosity on thermal and electrical properties of polycrystalline bulk ZrN prepared by spark plasma sintering. *Journal of Alloys and Compounds*, 432(12):7–10, 2007.

[14] H. Muta, K. Kurosaki, M. Uno, and S. Yamanaka. Thermophysical properties of several nitrides prepared by spark plasma sintering. *Journal of Nuclear Materials*, 389(1):186–190, 2009.

[15] Development status of metallic dispersion and non-oxide advanced and alternative fuels for power and research reactors. Report, International Atomic Energy Agency (IAEA), 2003.

[16] H. F. Jackson and W. E. Lee. *Properties and Characteristics of ZrC*, book section 2.13, pages 339–372. Comprehensive Nuclear Materials. Elsevier, Oxford, 2012.

[17] J.C. Hedge, J.W. Kopec, C. Kostenko, and J.L. Lang. Thermal properties of refractory alloys. *US Air Force Report ASD-TDR*, pages 63–597, 1963.

[18] J. Adachi, K. Kurosaki, M. Uno, and S. Yamanaka. Thermal and electrical properties of zirconium nitride. *Journal of Alloys and Compounds*, 399(12):242–244, 2005.

[19] E. Grigore, C. Ruset, X. Li, and H. Dong. Zirconium carbonitride films deposited by combined magnetron sputtering and ion implantation (CMSII). *Surface and Coatings Technology*, 204(1213):1889–1892, 2010.

[20] H. Berndt, A. Q. Zeng, H. R. Stock, and P. Mayr. Zirconium carbonitride films produced by plasma-assisted metal organic chemical vapour deposition. *Surface and Coatings Technology*, Part 1(7475):369–374, 1995.

[21] C. Hsin-Tien and H. Cheng-Chung. Low-pressure chemical vapor deposition of titanium and zirconium carbonitride thin films from $M(NEt_2)_4$ (M = Ti and Zr). *Materials Letters*, 16(4):194–199, 1993.

[22] I. A. Khan, S. Jabbar, T. Hussain, M. Hassan, R. Ahmad, M. Zakaullah, and R. S. Rawat. Deposition of zirconium carbonitride composite films using ion and electron beams emitted from plasma focus device. *Nuclear Instruments and Methods in Physics Research Section B: Beam Interactions with Materials and Atoms*, 268(13):2228–2234, 2010.

[23] W. Lengauer, S. Binder, K. Aigner, P. Ettmayer, A. Guillou, J. Debuigne, and G. Groboth. Solid state properties of group IVb carbonitrides. *Journal of Alloys and Compounds*, 217(1):137–147, 1995.

[24] K. Ohshima, J. Harada, M. Morinaga, P. Georgopoulos, and J. B. Cohen. Distortion-induced scattering due to vacancies in $NbC_{0.72}$. *Acta Crystallographica Section A*, 44(2):167–176, 1988.

[25] R.H.J. Hannink and M.V. Swain. Metastability of the martensitic transformation in a 12 molceria-zirconia alloy: I, deformation and fracture observations. *Journal of the American Ceramic Society*, 72(1):90–98, 1989.

[26] Philippe Bardelle and Dominique Warin. Mechanism and kinetics of the uranium-plutonium mononitride synthesis. *Journal of Nuclear Materials*, 188(0):36–42, 1992.

[27] A. Ortega, M. D. Alcala, and C. Real. Carbothermal synthesis of silicon nitride (Si_3N_4): Kinetics and diffusion mechanism. *Journal of Materials Processing Technology*, 195(13):224–231, 2008.

[28] A.W. Weimer, G.A. Eisman, D.W. Susnitzky, D.R. Beaman, and J.W. McCoy. Mechanism and kinetics of the carbothermal nitridation synthesis of α-silicon nitride. *Journal of the American Ceramic Society*, 80(11):2853–2863, 1997.

[29] J. David, G. Trolliard, M. Gendre, and A. Maitre. TEM study of the reaction mechanisms involved in the carbothermal reduction of zirconia. *Journal of the European Ceramic Society*, 33(1):165–179, 2013.

[30] G. W. Chinthaka Silva, A.A. Kercher, J.D. Hunn, R.C. Martin, G.E. Jellison, and H.M. Meyer. Characterization of zirconium carbides using electron microscopy, optical anisotropy, Auger depth profiles, X-ray diffraction, and electron density calculated by charge flipping method. *Journal of Solid State Chemistry*, 194(0):91–99, 2012.

[31] A.N. Christensen. A neutron diffraction investigation on single crystal of titanium carbide, titanium nitride and zirconium nitride. *Acta Chemica Scandinavica A*, 29:563–568, 1975.

[32] W. Lengauer. *Transition Metal Carbides, Nitrides, and Carbonitrides*, pages 202–252. Wiley-VCH Verlag GmbH, 2008.

[33] M.W. Chase. NIST-JANAF Themochemical Tables, Fourth Edition. *J. Phys. Chem. Ref. Data,*, Monograph 9:1–1951, 1998.

[34] D.S. Neel, S. Oglesby, and C.D. Pears. *The thermal properties of thirteen solid materials to 5000° F for their destruction temperatures.* WAAD technical documentary reportno. 60-924. Directorate of Materials and Processes, Aeronautical Systems Division, Air Force Systems Command, Wright-Patterson Air Force Base, Ohio, 1962. (Birmingham, AL.) "Project no. 7360, Task no. 73603." "Prepared under Contract no. AF 33 (616)-6312, by the Southern Research Institute, Birmingham, Alabama.".

[35] R. E. Taylor and J. Morreale. Thermal conductivity of titanium carbide, zirconium carbide, and titanium nitride at high temperatures. *Journal of the American Ceramic Society*, 47(2):69–73, 1964.

[36] Y. Arai, Y. Okamoto, and Y. Suzuki. Thermal conductivity of neptunium mononitride from 740 to 1600 k. *Journal of Nuclear Materials*, 211(3):248–250, 1994.

[37] Merja Pukari and Masahide Takano. Sintering and characterization of zrn and (dy,zr)n as surrogate materials for fast reactor nitride fuel. *Journal of Nuclear Materials*, 444(13):7 – 13, 2014.

[38] C.R. Stanek, K.J. McClellan, L.A. Morales, D.D. Byler, S.L. Voit, and J.B. Henderson. Thermal conductivity of polycrystalline zirconium nitride as a function of temperature, porosity, and oxygen impurity level. In *Advanced nuclear fuel cycles and systems (GLOBAL 2007)*. American Nuclear Society (ANS), 2007.

[39] J. Gan, Y. Yang, C. Dickson, and T. Allen. Proton irradiation study of GFR candidate ceramics. *Journal of Nuclear Materials*, 389(2):317–325, 2009.

[40] P.A. Demkowicz, K. Wright, J. Gan, D. A. Petti, T. Allen, and J. Blanchard. Evaluation of alternate materials for coated particle fuels for the Gas-Cooled Fast Reactor. Report, Idaho National Laboratory (INL), 2006.

[41] Gas-Cooled fast Reactor (GFR) FY04 Annual Report. Report, Idaho National Laboaratory (INL), 2004.

[1] Z. Su'Ud and H. Sekimoto. Design and safety aspect of lead and lead-bismuth cooled long-life small safe fast reactors for various fore configurations. *Journal of Nuclear Science and Technology*, 32(9):834–845, 1995.

[2] R. B. Matthews, K. M. Chidester, C. W. Hoth, R. E. Mason, and R. L. Petty. Fabrication and testing of uranium nitride fuel for space power reactors. *Journal of Nuclear Materials*, 151(3):345, 1988.

[3] Y. Arai and K. Minato. Fabrication and electrochemical behavior of nitride fuel for future applications. *Journal of Nuclear Materials*, 344(1-3):180–185, 2005.

[4] M. K. Meyer, R. Fielding, and J. Gan. Fuel development for gas-cooled fast reactors. *Journal of Nuclear Materials*, 371(13):281–287, 2007.

[5] W.E. Lee, M. Gilbert, S.T. Murphy, and R.W. Grimes. Opportunities for advanced ceramics and composites in the nuclear sector. *Journal of the American Ceramic Society*, 96(7):2005–2030, 2013.

[6] Y. Arai. *Nitride Fuel*, book section 3.02, pages 41–54. Comprehensive Nuclear Materials. Elsevier, Oxford, 2012.

[7] M. Burghartz, G. Ledergerber, H. Hein, R. R. van der Laan, and R. J. M. Konings. Some aspects of the use of ZrN as an inert matrix for actinide fuels. *Journal of Nuclear Materials*, 288(23):233–236, 2001.

[8] A. Ciriello, V. V. Rondinella, D. Staicu, J. Somers, O. Benes, R. Jardin, D. Bouxire, F. Wastin, and E. Colineau. Thermophysical characterization of ZrN and (Zr,Pu)N. *Journal of Alloys and Compounds*, 473(1-2):265–271, 2009.

[9] Y. Arai, M. Akabori, and K. Minato. Progress of nitride fuel cycle research for transmutation of minor actinides. In *Advanced nuclear fuel cycles and systems (GLOBAL 2007)*. American Nuclear Society, 2007. (Japan) [Japan Atomic Energy Agency - JAEA, Tokai-mura, Naka-gun, Ibaraki-ken, 319-1195].

[10] V. Basini, J. P. Ottaviani, J. C. Richaud, M. Streit, and F. Ingold. Experimental assessment of thermophysical properties of (Pu,Zr)N. *Journal of Nuclear Materials*, 344(1-3):186–190, 2005.

[11] Y. Arai and K. Nakajima. Preparation and characterization of PuN pellets containing ZrN and TiN. *Journal of Nuclear Materials*, 281(23):244–247, 2000.

[12] K. Minato, M. Akabori, M. Takano, Y. Arai, K. Nakajima, A. Itoh, and T. Ogawa. Fabrication of nitride fuels for transmutation of minor actinides. *Journal of Nuclear Materials*, 320(12):18–24, 2003.

[13] J. Adachi, K. Kurosaki, M. Uno, and S. Yamanaka. Effect of porosity on thermal and electrical properties of polycrystalline bulk ZrN prepared by spark plasma sintering. *Journal of Alloys and Compounds*, 432(12):7–10, 2007.

[14] H. Muta, K. Kurosaki, M. Uno, and S. Yamanaka. Thermophysical properties of several nitrides prepared by spark plasma sintering. *Journal of Nuclear Materials*, 389(1):186–190, 2009.

[15] Development status of metallic dispersion and non-oxide advanced and alternative fuels for power and research reactors. Report, International Atomic Energy Agency (IAEA), 2003.

[16] H. F. Jackson and W. E. Lee. *Properties and Characteristics of ZrC*, book section 2.13, pages 339–372. Comprehensive Nuclear Materials. Elsevier, Oxford, 2012.

[17] J.C. Hedge, J.W. Kopec, C. Kostenko, and J.L. Lang. Thermal properties of refractory alloys. *US Air Force Report ASD-TDR*, pages 63–597, 1963.

[18] J. Adachi, K. Kurosaki, M. Uno, and S. Yamanaka. Thermal and electrical properties of zirconium nitride. *Journal of Alloys and Compounds*, 399(12):242–244, 2005.

[19] E. Grigore, C. Ruset, X. Li, and H. Dong. Zirconium carbonitride films deposited by combined magnetron sputtering and ion implantation (CMSII). *Surface and Coatings Technology*, 204(1213):1889–1892, 2010.

[20] H. Berndt, A. Q. Zeng, H. R. Stock, and P. Mayr. Zirconium carbonitride films produced by plasma-assisted metal organic chemical vapour deposition. *Surface and Coatings Technology*, Part 1(7475):369–374, 1995.

[21] C. Hsin-Tien and H. Cheng-Chung. Low-pressure chemical vapor deposition of titanium and zirconium carbonitride thin films from $M(NEt_2)_4$ (M = Ti and Zr). *Materials Letters*, 16(4):194–199, 1993.

[22] I. A. Khan, S. Jabbar, T. Hussain, M. Hassan, R. Ahmad, M. Zakaullah, and R. S. Rawat. Deposition of zirconium carbonitride composite films using ion and electron beams emitted from plasma focus device. *Nuclear Instruments and Methods in Physics Research Section B: Beam Interactions with Materials and Atoms*, 268(13):2228–2234, 2010.

[23] W. Lengauer, S. Binder, K. Aigner, P. Ettmayer, A. Guillou, J. Debuigne, and G. Groboth. Solid state properties of group IVb carbonitrides. *Journal of Alloys and Compounds*, 217(1):137–147, 1995.

[24] K. Ohshima, J. Harada, M. Morinaga, P. Georgopoulos, and J. B. Cohen. Distortion-induced scattering due to vacancies in $NbC_{0.72}$. *Acta Crystallographica Section A*, 44(2):167–176, 1988.

[25] R.H.J. Hannink and M.V. Swain. Metastability of the martensitic transformation in a 12 molceria-zirconia alloy: I, deformation and fracture observations. *Journal of the American Ceramic Society*, 72(1):90–98, 1989.

[26] Philippe Bardelle and Dominique Warin. Mechanism and kinetics of the uranium-plutonium mononitride synthesis. *Journal of Nuclear Materials*, 188(0):36–42, 1992.

[27] A. Ortega, M. D. Alcala, and C. Real. Carbothermal synthesis of silicon nitride (Si_3N_4): Kinetics and diffusion mechanism. *Journal of Materials Processing Technology*, 195(13):224–231, 2008.

[28] A.W. Weimer, G.A. Eisman, D.W. Susnitzky, D.R. Beaman, and J.W. McCoy. Mechanism and kinetics of the carbothermal nitridation synthesis of α-silicon nitride. *Journal of the American Ceramic Society*, 80(11):2853–2863, 1997.

[29] J. David, G. Trolliard, M. Gendre, and A. Maitre. TEM study of the reaction mechanisms involved in the carbothermal reduction of zirconia. *Journal of the European Ceramic Society*, 33(1):165–179, 2013.

[30] G. W. Chinthaka Silva, A.A. Kercher, J.D. Hunn, R.C. Martin, G.E. Jellison, and H.M. Meyer. Characterization of zirconium carbides using electron microscopy, optical anisotropy, Auger depth profiles, X-ray diffraction, and electron density calculated by charge flipping method. *Journal of Solid State Chemistry*, 194(0):91–99, 2012.

[31] A.N. Christensen. A neutron diffraction investigation on single crystal of titanium carbide, titanium nitride and zirconium nitride. *Acta Chemica Scandinavica A*, 29:563–568, 1975.

[32] W. Lengauer. *Transition Metal Carbides, Nitrides, and Carbonitrides*, pages 202–252. Wiley-VCH Verlag GmbH, 2008.

[33] M.W. Chase. NIST-JANAF Themochemical Tables, Fourth Edition. *J. Phys. Chem. Ref. Data,*, Monograph 9:1–1951, 1998.

[34] D.S. Neel, S. Oglesby, and C.D. Pears. *The thermal properties of thirteen solid materials to 5000°F for their destruction temperatures.* WAAD technical documentary reportno. 60-924. Directorate of Materials and Processes, Aeronautical Systems Division, Air Force Systems Command, Wright-Patterson Air Force Base, Ohio, 1962. (Birmingham, AL.) "Project no. 7360, Task no. 73603." "Prepared under Contract no. AF 33 (616)-6312, by the Southern Research Institute, Birmingham, Alabama.".

[35] R. E. Taylor and J. Morreale. Thermal conductivity of titanium carbide, zirconium carbide, and titanium nitride at high temperatures. *Journal of the American Ceramic Society*, 47(2):69–73, 1964.

[36] Y. Arai, Y. Okamoto, and Y. Suzuki. Thermal conductivity of neptunium mononitride from 740 to 1600 k. *Journal of Nuclear Materials*, 211(3):248–250, 1994.

[37] Merja Pukari and Masahide Takano. Sintering and characterization of zrn and (dy,zr)n as surrogate materials for fast reactor nitride fuel. *Journal of Nuclear Materials*, 444(13):7 – 13, 2014.

[38] C.R. Stanek, K.J. McClellan, L.A. Morales, D.D. Byler, S.L. Voit, and J.B. Henderson. Thermal conductivity of polycrystalline zirconium nitride as a function of temperature, porosity, and oxygen impurity level. In *Advanced nuclear fuel cycles and systems (GLOBAL 2007)*. American Nuclear Society (ANS), 2007.

[39] J. Gan, Y. Yang, C. Dickson, and T. Allen. Proton irradiation study of GFR candidate ceramics. *Journal of Nuclear Materials*, 389(2):317–325, 2009.

[40] P.A. Demkowicz, K. Wright, J. Gan, D. A. Petti, T. Allen, and J. Blanchard. Evaluation of alternate materials for coated particle fuels for the Gas-Cooled Fast Reactor. Report, Idaho National Laboratory (INL), 2006.

[41] Gas-Cooled fast Reactor (GFR) FY04 Annual Report. Report, Idaho National Laboaratory (INL), 2004.

List of Figures

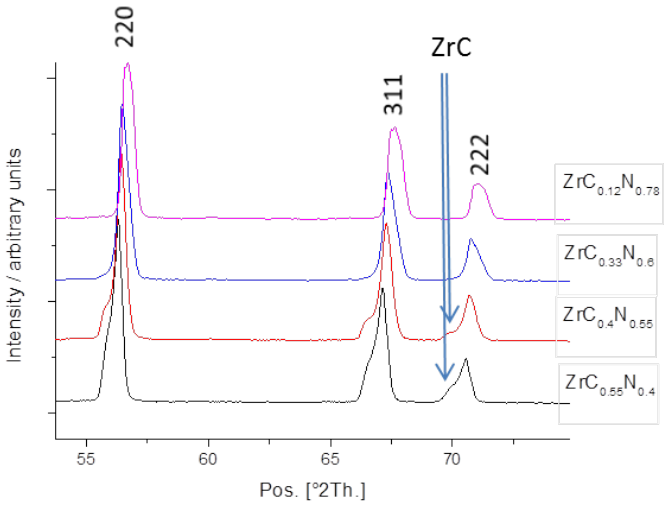

Figure 1: XRD of ZrC_xN_y powders before sintering

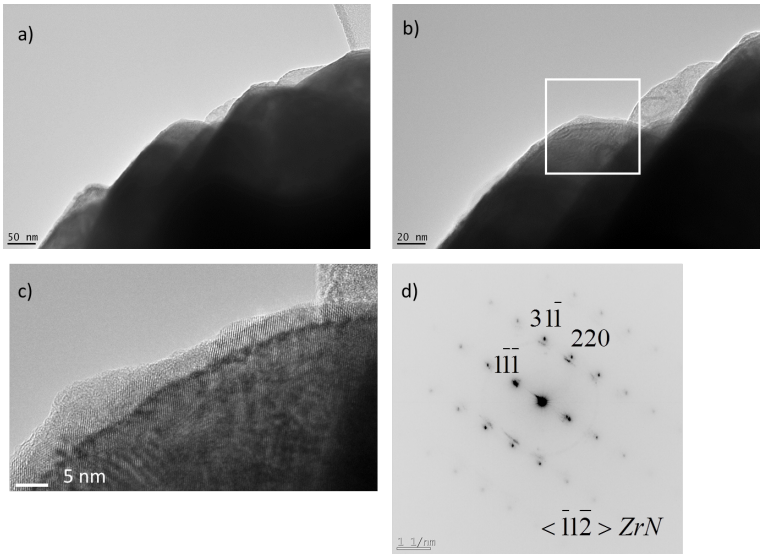

Figure 2: a,b) Bright-field TEM of region of powder from $ZrC_{0.67}N_{0.33}$, c) image of SAED area. d) SAED pattern

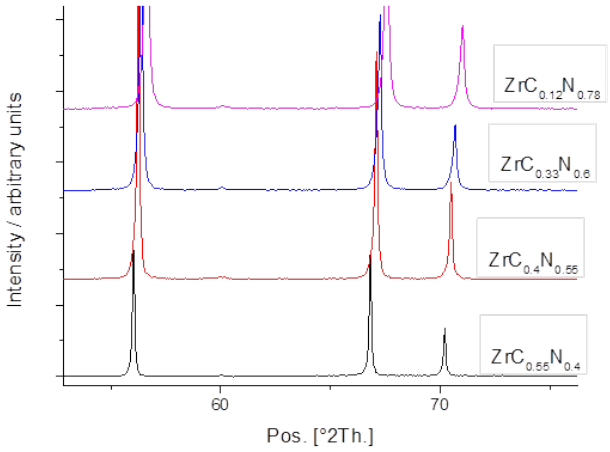

Figure 3: XRD of ZrC_xN_yceramic pellets after sintering

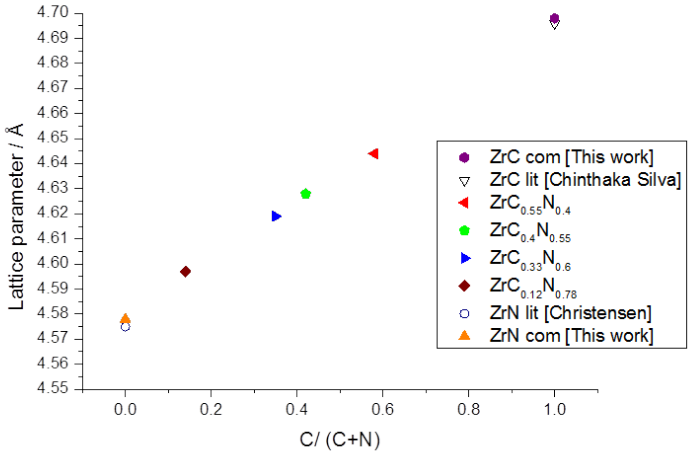

Figure 4: Lattice parameters of ZrC, ZrN and ZrC_xN_y ceramics as a function of [C]/[C]+[N] with literature values of ZrC and ZrN [30, 31]

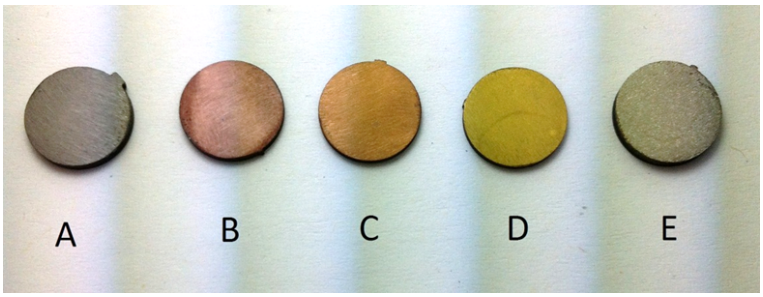

Figure 5: Photograph of 10mm ceramic pellets A) commercial ZrC, B) $ZrC_{0.4}N_{0.55}$, C) $ZrC_{0.33}N_{0.6}$, D) $ZrC_{0.12}N_{0.78}$, E) ZrN commercial

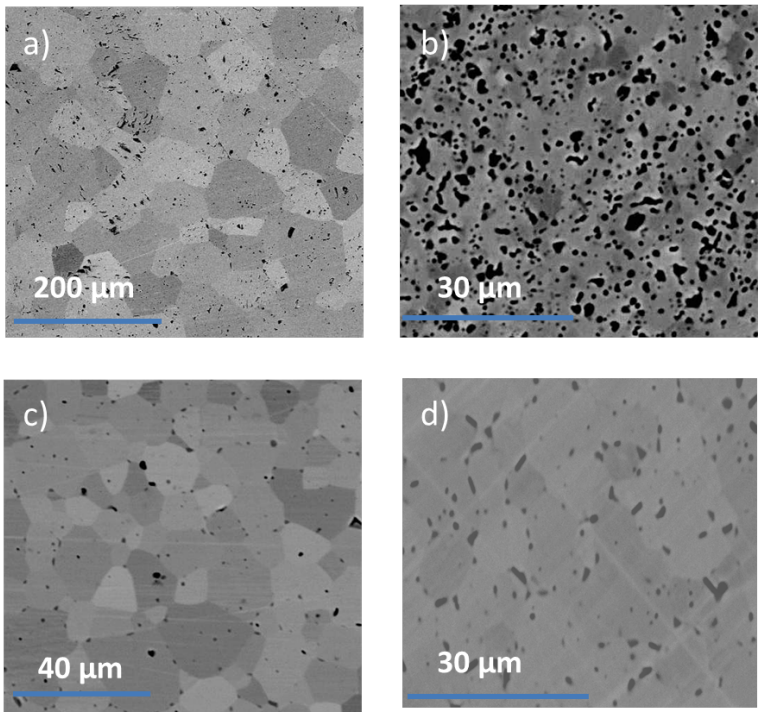

Figure 6: BS electron images of ceramic pellets, a) commercial ZrN, b) commercial ZrC, c) $ZrC_{0.55}N_{0.4}$d) $ZrC_{0.12}N_{0.78}$

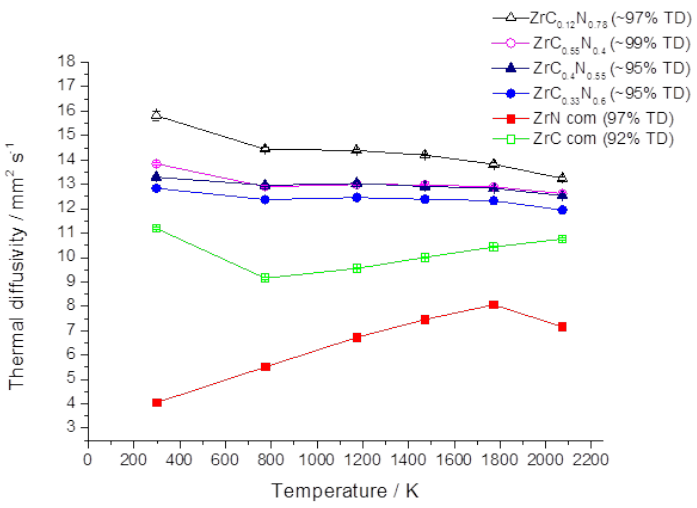

Figure 7: Thermal diffusivity of ceramics prepared from commercial and fabricated powders

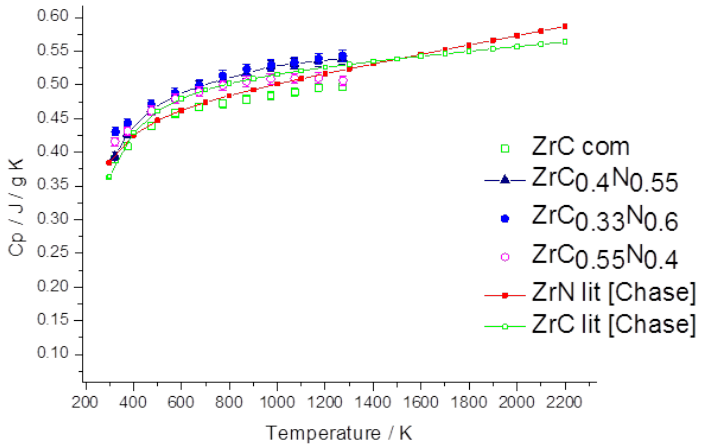

Figure 8: Temperature dependence of heat capacities of ceramics produced in this work, together with literature values [33]

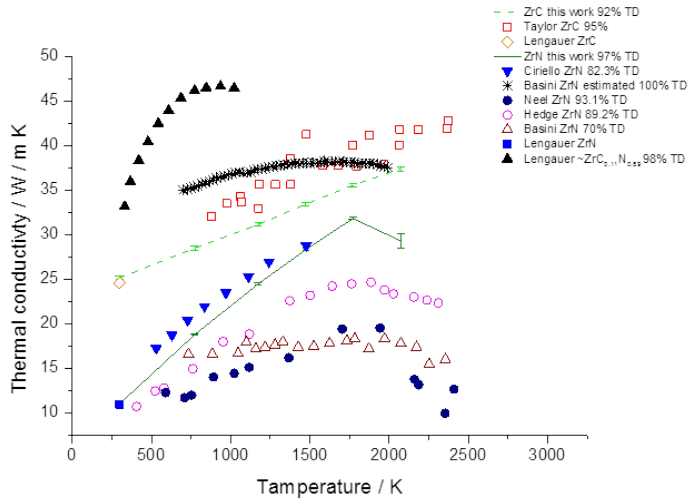

Figure 9: Temperature dependence of thermal conductivity of ZrC and ZrN, together with literature data [8, 10, 17, 23, 32, 34, 35]

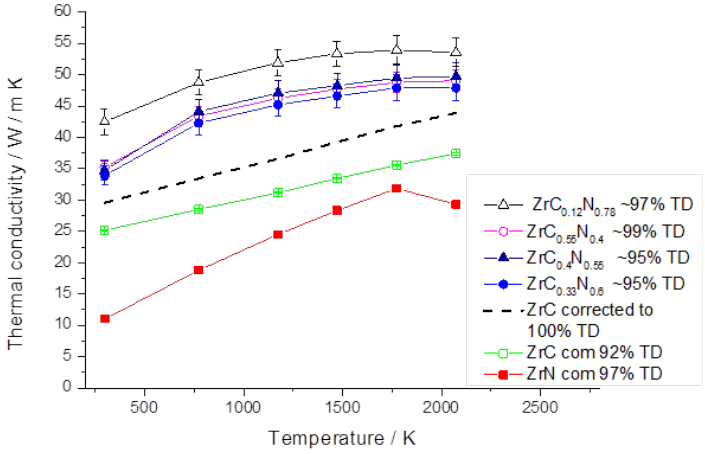

Figure 10: Temperature dependence of thermal conductivity of ZrC, ZrN and ZrC_xN_yceramics

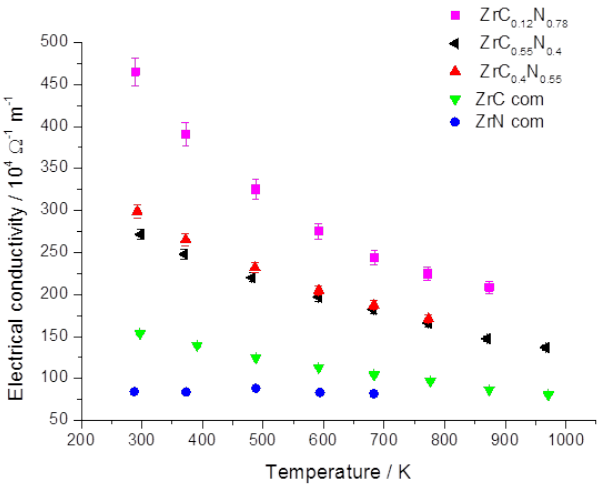

Figure 11: Temperature dependence of electrical conductivity of ZrC, ZrN and ZrC_xN_yceramics

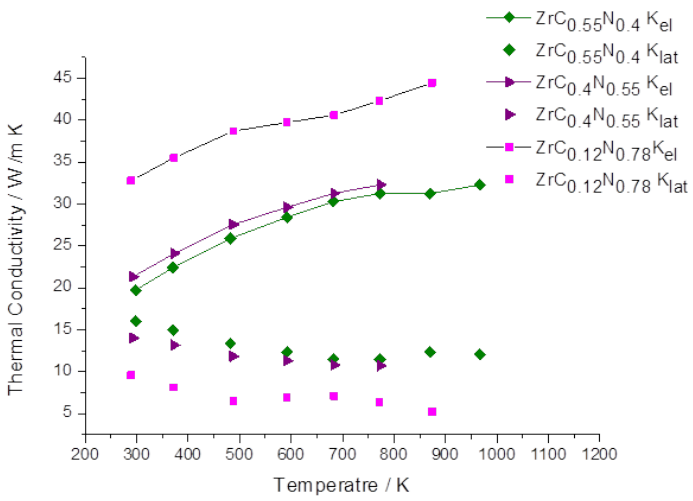

Figure 12: Temperature dependence of electrical and phonon contribution to thermal conductivities of ZrC_xN_yceramics

List of Tables

Sample	Starting C/Zr mol ratio	Dwell time / h	Dwell temperature / K	Atmosphere	at% C	at% N	Stoichiometry
1Zr-2.7C	2.7	4	2073	Ar	44.42±1.82	2.42 ±0.39	$ZrC_{0.89}N_{0.04}$
1Zr-3C	3	4	2073	Ar	49.76±6.06	1.99 ±0.57	$ZrC_{1.00}N_{0.04}$
ZrC commercial	-	-	-	-	44.67±3.24	2.35 ±0.44	$ZrC_{0.89}N_{0.04}$
ZrN commercial	-	-	-	-	0.19 ± 0.12	43.11 ±0.64	$ZrN_{0.86}$
ZrCN-1	3	8	1873	10% H_2 - 90% N_2	28.52 ±0.78	18.00 ±0.29	$ZrC_{0.36}N_{0.57}$
ZrCN-2	2.7	8	1873	10% H_2 - 90% N_2	25.03 ±0.26	20.72 ±0.42	$ZrC_{0.50}N_{0.45}$
ZrCN-3	3	24	1800	10% H_2 - 90% N_2	12.09 ±0.49	34.86 ±0.15	$ZrC_{0.25}N_{0.70}$
ZrCN-4	3	24	1873	10% H_2 - 90% N_2	6.04 ±0.25	39.23 ±0.22	$ZrC_{0.12}N_{0.78}$

Table 1: Carbon and nitrogen analysis of nitrided powders using oxidation method

Sample	wt% C	at% C	wt% N	at% N	at% O	Stoichiometry
1Zr-2.7C	11.23 ±0.20	46.78	-	-	-	$ZrC_{0.93}$
1Zr-3C	12.35 ±0.22	51.47	-	-	-	$ZrC_{1.02}$
ZrCN-1[1]	4.84 ±0.08	26.98	7.39±0.10	26.96	3.43	$ZrC_{0.4}N_{0.55}O_{0.06}$
ZrCN-2[1]	6.36 ±0.11	27.50	5.47 ±0.13	20.25	2.65	$ZrC_{0.54}N_{0.4}O_{0.04}$
ZrCN-3[1]	3.90 ±0.07	16.54	8.22 ±0.15	29.90	4.83	$ZrC_{0.33}N_{0.6}O_{0.08}$
ZrCN-4[2]	1.89 ±0.03	-	-	-	-	-

Table 2: Carbon, nitrogen and oxygen chemical analysis of nitrided powders using combustion analysis, 1) Pellet analysed, 2) Powder analysed

Sample	Particle size / μm	Density / g cm^{-3}	%TD	Average grain size / μm
ZrN com	1–2^a	7.08 ±0.02	97.0 ±0.3	$\sim$ 100^c
ZrC com	$\leq$5^a	6.20 ±0.02	92.1 ±0.3	$\sim$ 5^c
$ZrC_{0.55}N_{0.4}$	1–5^b	6.90 ±0.01	$\backsimeq$ 99%^{b}	10–30^c
$ZrC_{0.4}N_{0.55}$	1–5^b	6.95 ±0.07	$\geq$95	-
$ZrC_{0.33}N_{0.6}$	1–5^b	7.00 ±0.07	$\geq$95	-
$ZrC_{0.12}N_{0.78}$	1–5^b	7.06 ±0.04	$\backsimeq$ 97%^{b}	10–30 ^{c}

Table 3: Bulk properties of hot pressed ceramic pellets, ^{a}- Manufacturers analysis ^{b}- Measured by SEM ^{c}- Average line intercept, TD = theoretical density from manufacturers

Sample	K_{el}/ $Wm^{-1}K^{-1}$	K_{tot}/ $Wm^{-1}K^{-1}$	% K_{el}/ K_{tot}
ZrC com	11.1 ±0.1	23.3 ±0.9	47.6
$ZrC_{0.55}N_{0.4}$	19.7 ± 0.5	35.2 ±1.2	56.0
$ZrC_{0.4}N_{0.55}$	21.3±0.6	34.7 ±1.5	61.3
$ZrC_{0.12}N_{0.78}$	32.8 ±1.1	42.4 ±2.1	77.3
ZrN com	5.9 ±0.1	11.0 ±0.4	53.6

Table 4: Percentage contribution of K_{el} to total thermal conductivity of ZrC, ZrN and ZrC_xN_yceramics